On the localized surface plasmon resonance modes in nanoporous gold films

Detsi, Eric; Salverda, Mart; Onck, Patrick R.; De Hosson, Jeff Th. M.

Published in:
Journal of Applied Physics

DOI:
10.1063/1.4862440

On the localized surface plasmon resonance modes in nanoporous gold films

Eric Detsi, Mart Salverda, Patrick R. Onck, and Jeff Th. M. De Hosson

Citation: Journal of Applied Physics **115**, 044308 (2014); doi: 10.1063/1.4862440
View online: https://doi.org/10.1063/1.4862440
View Table of Contents: http://aip.scitation.org/toc/jap/115/4
Published by the American Institute of Physics

On the localized surface plasmon resonance modes in nanoporous gold films

Eric Detsi, Mart Salverda, Patrick R. Onck, and Jeff Th. M. De Hosson[a)]
Department of Applied Physics, Zernike Institute for Advanced Materials, University of Groningen, Nijenborgh 4, 9747 AG Groningen, The Netherlands

(Received 15 October 2013; accepted 6 January 2014; published online 27 January 2014)

This work concentrates on the relation between plasmonic modes and the microstructure of nanoporous gold films. Based on experiments and computational analyses, we conclude that ligament as well as pore sizes need to be taken into account for an adequate physical description of the optical performance of a disordered nanoporous metal film as a function of its detailed microstructure. © *2014 AIP Publishing LLC*. [http://dx.doi.org/10.1063/1.4862440]

I. INTRODUCTION

An intriguing phenomenon is the enhanced visible light transmission through a nanoporous gold (NPG) film. This is called the Extraordinary Optical Transmission (EOT) phenomenon,[1,2] which is attributed to the localized surface plasmon resonance in nanoporous media.[3] This enhanced transmission performance is characterized by two peaks in the optical spectra of the free-standing NPG films. First, a long-wavelength peak commonly associated with the localized surface plasmon resonance (LSPR) in the film.[3] Upon *increasing* pore size the long-wavelength peak has been reported to redshift.[3] Second, a short-wavelength peak that is attributed to the resonant absorption in the film,[3] i.e., coupling of the excited LSPR mode with light.[4,5] The position of this short-wavelength peak is supposed to be *independent* of the size of ligaments and pores.[3] The work reported in this paper is aimed at investigating whether the characteristic size of the ligaments, or the characteristic size of the pores, is sufficient for an adequate description of the optical behavior of disordered nanoporous metal films. We will show that it is essential that both ligament and pore sizes are taken into account. In contrast to the aforementioned redshift of the long-wavelength peak with increasing pore (or ligament) size,[3] experimentally we have observed a redshift followed by a blueshift of this long-wavelength peak with increasing pore (or ligament) size. Experimental and computational methods based on Bruggeman's effective medium theory were exploited to support our findings. Our results will contribute to a better understanding and characterization of the plasmonic modes in disordered nanoporous metals.

II. MATERIALS AND EXPERIMENTAL PROCEDURES

NPG films were synthesized from white Au leafs precursors (Linova, Netherlands) with compositions $Au_{15}Ag_{85}$ (at. %) and $Au_{35}Ag_{65}$ (at. %), both having an average thickness of 100 nm. Ag was chemically removed from these precursors by dissolution in concentrated nitric acid (65%) at room temperature.[6,7] The final residual Ag content in all dealloyed structures was maintained below ~5 at. %. This is because a minimum residual Ag content in NPG is desirable for accurate optical data. Indeed, the position of the localized surface plasmon resonance peak for pure Au is different from that of pure Ag. Consequently, the higher the residual Ag content in NPG, the closer its localized surface plasmon resonance peak comes to that of Ag.[8]

Since we concentrate on the optical spectra as a function of the pore and ligament sizes, a wide range feature sizes is desirable. These feature sizes were obtained by coarsening the dealloyed NPG films in concentrated nitric acid, either at room temperature from 10 min to 30 h, or at 75 °C from 5 min to 8 h. The growth of the pores and ligaments during acid and thermal treatments is driven by the minimization of the interface energy via reduction of the interface surface area.[7]

The optical spectra of the NPG films were investigated using either a standard spectrophotometer (Perkin-Elmer Lambda 900 UV-Vis-NIR Spectrometer),[8] for large specimen films, or a microspectrophotometer for small specimen films. As surrounding media, we used air or water. For measurement in air, a nanoporous gold film is simply deposited onto a glass plate substrate. For measurement with water as surrounding medium, the nanoporous gold film is sandwiched between two glass plates, and water is introduced by capillary absorption.

In order to get a clear insight into our experimental data, the optical spectra of NPG films were further analyzed using the Bruggeman's effective medium theory.

III. EXPERIMENTAL RESULTS AND DISCUSSIONS

During chemical dealloying, a white Au leaf becomes entirely porous within the first 10 min in concentrated nitric acid,[3] and the corresponding pores and ligaments sizes are smaller than 10 nm. At this stage, however, the residual Ag in NPG films is about ~10 at. % as investigated by energy dispersive x-ray spectroscopy (EDS). In order to reduce this residual Ag down to ~5% or lower, NPG films are kept in acid at room temperature for 30 min, resulting in features sizes of about ~15 nm for the precursor with composition $Au_{35}Ag_{65}$ (at. %) and ~10 nm for the one with composition $Au_{15}Ag_{85}$ (at. %). These represent our starting materials.

A first set of experiments was performed with NPG films obtained from the precursor with elemental

a)j.t.m.de.hosson@rug.nl

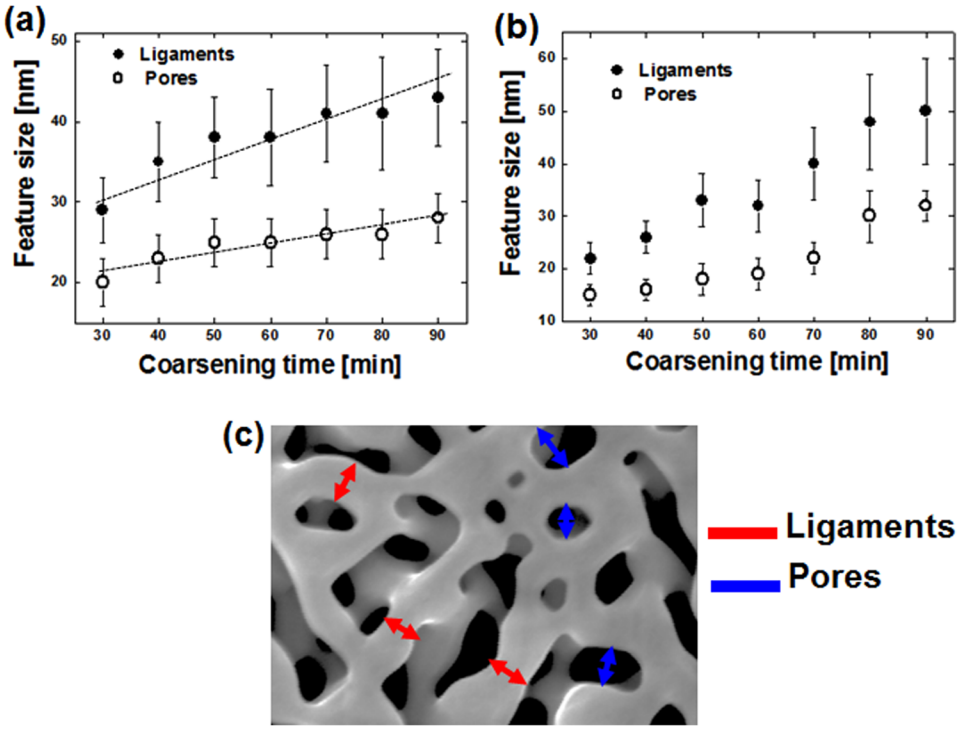

FIG. 1. (a) and (b) Typical changes in size of ligament and pore as a function of the coarsening time for two different sets of NPG films. It can be seen from the slopes of the linear fits in (a) that ligaments grow faster than pores. (c) Illustration of how the average size of the ligaments and pores were measured.

composition $Au_{35}Ag_{65}$ (at. %). These porous films were coarsened in acid at room temperature for various time intervals ranging from 10 min to 30 h. The corresponding average[9] feature sizes vary between ~15 and ~60 nm. Figs. 1(a) and 1(b) display typical changes in feature sizes as a function of the coarsening time, for two different sets of NPG films. It is seen that: First, the growth of pores and ligaments is not reproducible during acid coarsening. In particular, feature sizes in Fig. 1(a) are much bigger than those in Fig. 1(b); Second, the growth rate of the pores is different from that of the ligaments, in accordance with our previous publication.[9] For instance in Fig. 1(a), ligaments grow faster than pores as depicted by the slopes of the corresponding linear fits. This behavior highlights the necessity of taking into account both pore size and ligament size when studying the optical spectra of NPG films as a function of their feature sizes. It is emphasized that the abovementioned microstructural changes that we describe here as a separate variation of ligament size versus pore size is actually well known as a densification of nanoporous gold during coarsening. In other words, the structural characteristics may equivalently be described in terms of independent pore and ligament sizes (as is the case in this article), or in terms of ligament size and solid fraction. Note that in Figs. 1(a) and 1(b) the size of the pore is smaller than that of the ligament. It has to do with the way that these feature sizes are defined, as illustrated in Fig. 1(c). Although it is easy to measure the size of the ligaments from scanning electron micrographs (i.e., the average diameter of the struts)[9] it is not so straightforward to measure the size of the pores because of the very irregular morphology. Therefore, only pores with a quasi-regular geometry were measurable.

A second set of experiments was performed with NPG films with the same composition $Au_{35}Ag_{65}$ (at. %), but coarsened in fresh acid at 75 °C for various time intervals ranging from 5 min to 8 h. The thermal coarsening in acid is faster than coarsening at room temperature, i.e., ligament diameters of ~60 nm are readily achieved within 2 h. Figs. 2(a) and 2(b) display two typical microstructures of NPG at the same magnification and scale, before and after thermal coarsening in acid. It is evident from Fig. 2(b) that the final

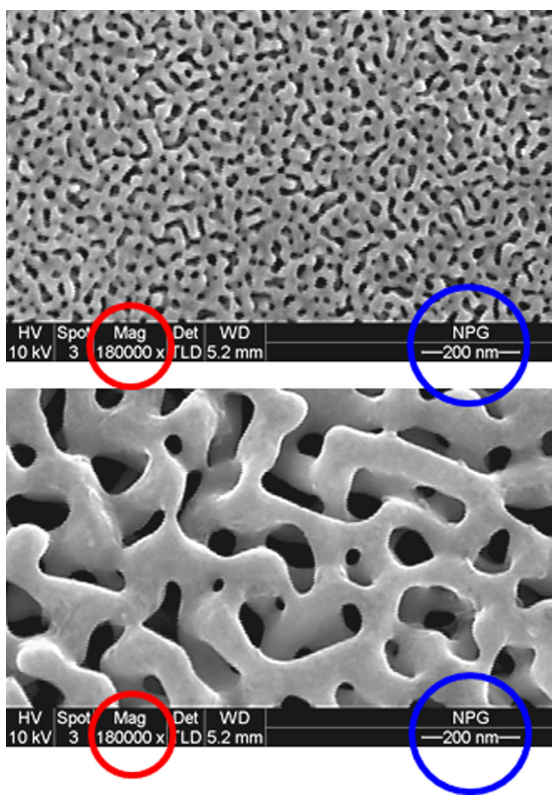

FIG. 2. Microstructures of NPG at the same magnification, (a) before and (b) after thermal coarsening in acid.

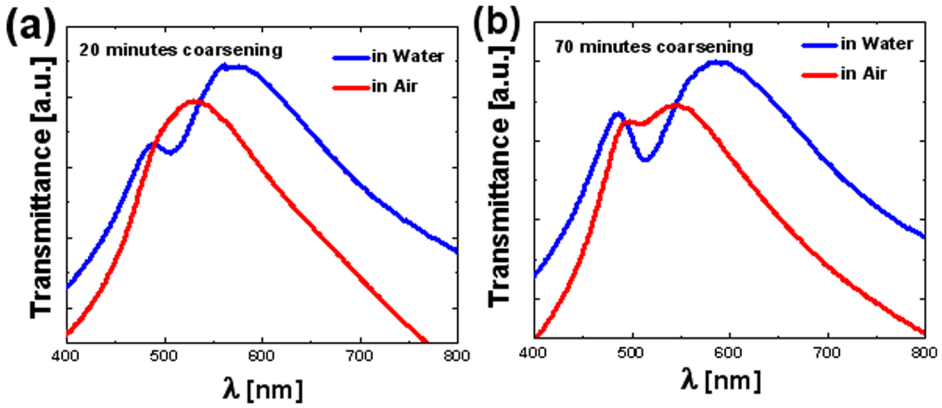

FIG. 3. Transmission spectra of two NPG films with different feature sizes measured first in air and afterwards in water. Feature sizes are smaller in (a) than in (b). The short- and long-wavelengths peaks are separated when water is used as surrounding medium; they overlap when measurements are performed with air as surrounding medium.

ligament sizes are comparable to the film thickness, meaning that the self-similar coarsening that has been observed in several other studies on bulk samples of nanoporous gold cannot be expected in the present material.

In order to choose an appropriate medium for the investigation of the plasmonic modes in the 2 NPG films, the optical spectra were collected in water and in air during preliminary experiments. Figs. 3(a) and 3(b) display the transmission spectra of two NPG specimens with different feature sizes, collected first in air and afterwards in water. It is seen that the short- and long-wavelength peaks are separated when a solvent is used (water as surrounding medium), and overlap when no solvent is used (air as surrounding medium). Therefore, it is appropriate to further concentrate on measurements with water as surrounding medium, where the two plasmonic peaks are clearly pronounced.

Rather than a permanent redshift of the long-wavelength peak with increasing pore or ligament size,[3] we report here a striking result, namely, a blueshift of this long-wavelength peak with increasing ligament (or pore) size. Fig. 4(a) shows the transmission spectra of six NPG films with different average ligament sizes obtained from the precursor with composition $Au_{35}Ag_{65}$ (at. %) and coarsened in acid at room temperature. It is seen that the long-wavelength peak initially shifts to the red with increasing ligament diameter.[3] However, as the ligament increases further, this peak shifts back to blue. The position of the long-wavelength peak as a function of the average ligament diameter is displayed in Fig. 4(b).

The spectra shown in Fig. 4(a) were collected using a spectrophotometer with incident light beam having a spot size of a few millimeters square. Consequently, the sample area exposed to the light beam is relatively large, and this may suggest that local variations in the microstructure (i.e., feature sizes) of NPG as depicted by the error bars in Figs. 1(a) and 1(b) can contribute to the blueshift of the long-wavelength peak. However, this is not the case because measurements of local optical spectra of NPG films using a microspectrophotometer, where the light beam has only a spot size of a few micrometers squared, also reveal a blueshift of the long-wavelength peak with increasing ligament diameter. Typical local spectra collected using the microspectrophotometer are shown in Fig. 5(a), and the corresponding peak position as a function of the ligament size is shown in Fig. 5(b). Here, the NPG films were obtained from the precursor with composition $Au_{15}Ag_{85}$ (at. %) and the spectra were collected with air as surrounding medium.

Another interesting result is the blueshift of the short-wavelength peak with increasing feature sizes. So far, in literature this peak has been reported to be independent on the size of the ligaments and pores.[3] However, it can be seen from Fig. 6(a) that the short-wavelength peak shifts slightly to the blue with increasing aspect ratio, while in the meantime the long-wavelength peak shifts to the red. The spectra in Fig. 6(a) were collected on NPG films made from the precursor with composition $Au_{35}Ag_{65}$ (at. %) and coarsened at 75 °C in acid; it is illustrated in Fig. 6(b) how the ARs of the ligaments are determined.

The simultaneous shifts of the two peaks in opposite directions, with increasing aspect ratio (AR), are specific to the optical spectra of metal nanorods. In metallic nanorods,

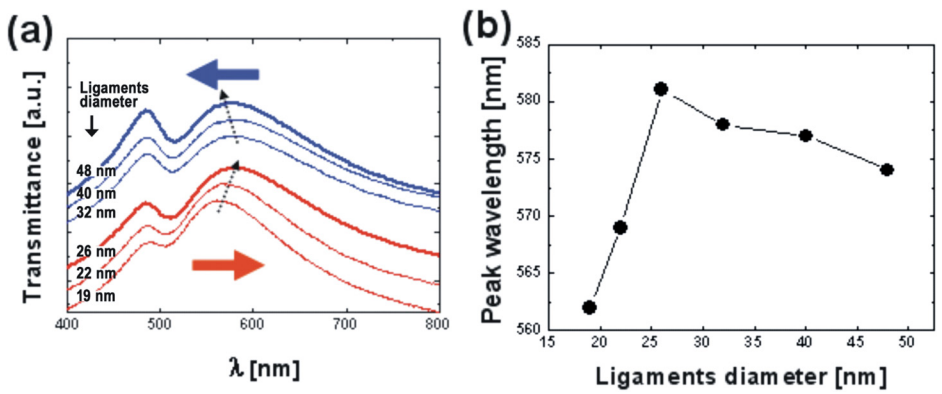

FIG. 4. (a) Transmission spectra of six NPG films having different average ligament sizes. The long-wavelength peak initially shifts to the red with increasing ligament diameter. As the ligament diameter increases further, this peak shifts back to the blue. (b) Position of the long-wavelength peak as a function of the average ligament diameter. These optical spectra were collected with water as surrounding medium. The measuring light beam has a spot size of a few mm^2, and the NPG films were made from the precursor with composition $Au_{35}Ag_{65}$ (at. %).

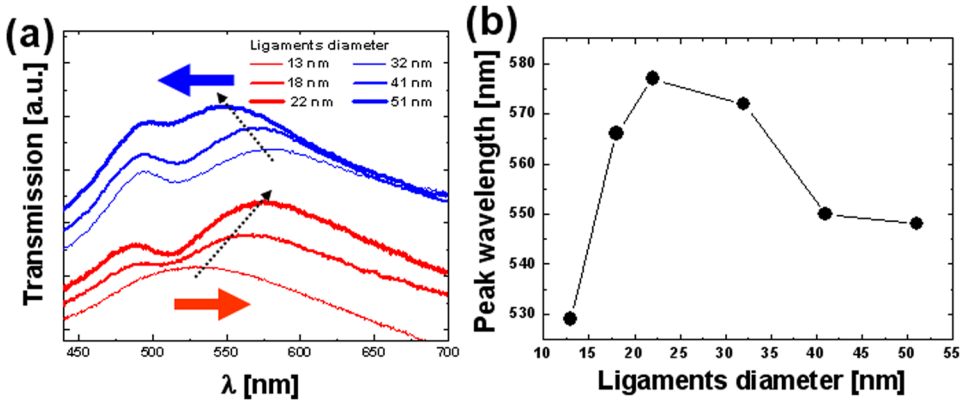

FIG. 5. (a) and (b) Identical to Figs. 4(a) and 4(b) but here the optical spectra are collected in air, the measuring light beam has a spot size of a few μm^2 and the NPG films are made from the precursor with composition $Au_{15}Ag_{85}$ (at. %).

the long-wavelength peak is well-known to originate from the longitudinal LSPR (oscillation of electrons along the major axis of the nanorods);[10] and this peak shifts to the red with increasing AR of the nanorods;[11] in contrast, the short-wavelength peak comes from the transverse LSPR in the nanorods (oscillation of electrons perpendicular to the major axis of the nanorods);[10] and this peak shifts slightly to the blue with increasing nanorods' AR.[11] These similarities between disordered NPG films and those of metal nanorods clearly suggest that the pseudo-aspect ratio of the ligaments (AR or η), which we define as the ratio of the average ligament length to the average ligament diameter (i.e., the average diameter of the struts), is a suitable structural parameter for the characterization of the optical spectra of disordered nanoporous metals films. Furthermore, as we have mentioned above, ligaments and pores do not evenly grow during coarsening. Fig. 7(a) shows that both ligament and pore sizes increase monotonously during coarsening, whereas the ratio does not. When the plasmonic peak positions such as those in Figs. 4(b) and 5(b) are plotted as a function of the AR, instead of just as a function of the ligament (or pore) size, the blueshift of the long-wavelength peak disappears: a monotone redshift of this long-wavelength peak with increasing AR is observed. This is illustrated by the plots in Figs. 7(b) and 7(c). In Sec. IV, the AR parameter will be used further to investigate the optical spectra of NPG films from an appropriate theoretical model.

IV. COMPUTATIONAL APPROACH

A popular model for the computation of the optical spectra of rod-shape metallic nanoparticles dispersed in a solvent is given by the Gans theory, also known as the modified Mie theory for spherical nanoparticles.[10,11] In the case of nanostructures with complex shapes, the Maxwell-Garnett (MG) effective medium theory,[12–14] a general approach to the Mie and Gans theories, is more appropriate for the computation of optical spectra. However, the MG effective medium theory deals with nanoparticles that are isolated (i.e., not interconnected) in the matrix of the surrounding medium.[12] Therefore the MG theory is not applicable to the interconnected ligaments in NPG films. In contrast to the MG approach, nanoparticles in a surrounding medium are allowed to touch each other in the Bruggeman (BM) effective medium theory.[12] The BM approach is more applicable to the ligaments in nanoporous metals and will be exploited in this section for the computation of the optical spectra of our NPG films.

As starting point, the optical properties of a given material, namely, its refractive index n and its absorption coefficient k, are related to the complex dielectric function ε of that material by the following relation:[10,12,13]

$$\varepsilon = (n + ik)^2 = \varepsilon' + i\varepsilon''. \quad (1)$$

In Eq. (1), ε' and ε'' are the real and imaginary part of the complex dielectric function, respectively. Knowing ε' and ε'',

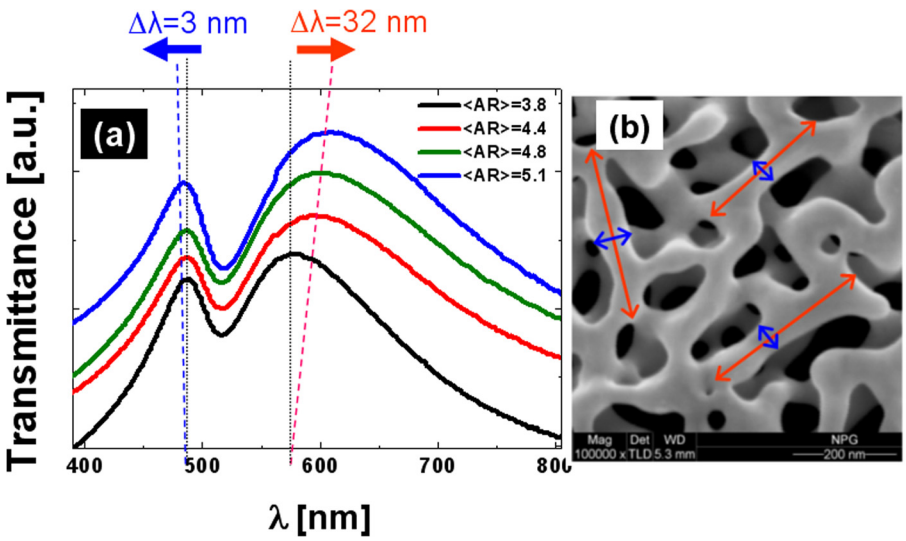

FIG. 6. Simultaneous shifts of the two plasmonic peaks in opposite directions. (a) The short-wavelength peak shifts slightly to the blue (up to 3 nm), while in the meantime the long-wavelength peak shifts to the red (up to 32 nm). The AR is defined as the ratio of the average ligament length to the average ligament diameter. (b) Illustration of how ligament length and diameter are measured.

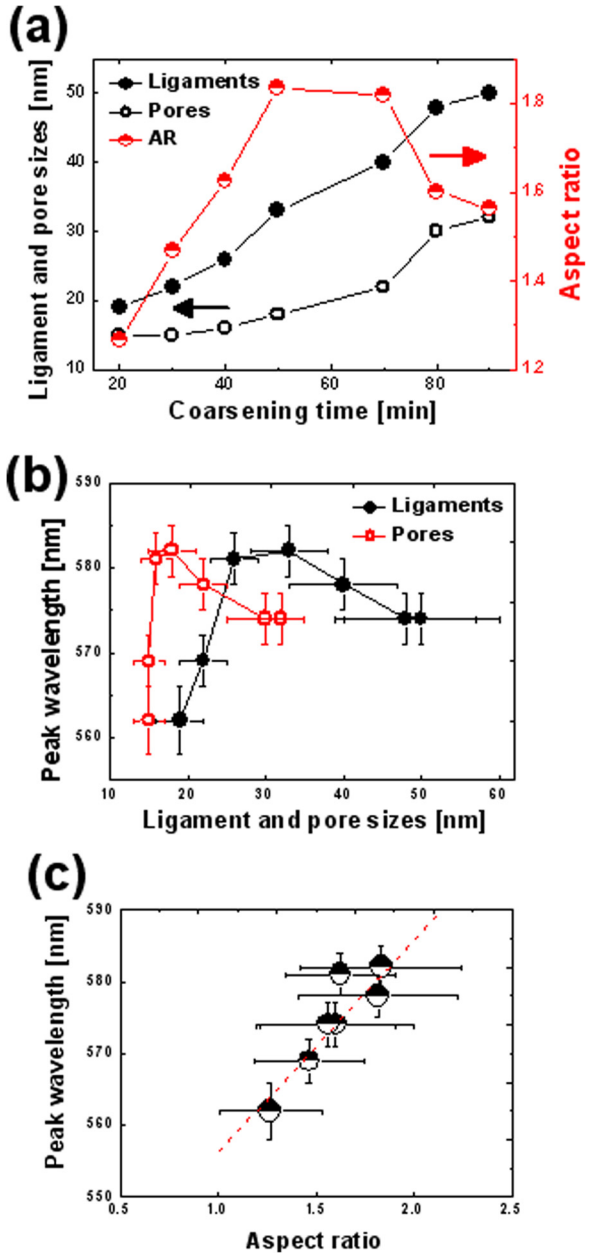

FIG. 7. (a) Both ligament and pore sizes increase monotonously during coarsening, but the ratio of the ligament to pore size does not. (b) The long-wavelength peak plotted as a function of the ligament or pore size shifts to the red and blue with increasing feature size. (c) The long-wavelength peak plotted as a function of the AR monotonously shifts to the red with increasing AR.

one can deduce the index of refraction n and the absorption coefficient k. The transmittance spectrum T of the material can then be computed from n and k in the case of normal incident light beam according to the following relations:[13]

$$T = \left[1 - \frac{(n-1)^2 + k^2}{(n+1)^2 + k^2}\right]^2 \exp\left(\frac{-4\pi k d}{\lambda}\right). \quad (2)$$

In Eq. (2), d and λ represent the thickness of the material and the wavelength of the incoming light, respectively. Note that ε' and ε'' in Eq. (1) varies with λ; consequently, n, k, and T are functions of the wavelength λ as well. The knowledge of the real and imaginary part ε' and ε'' of the complex dielectric function of the material is the only prerequisite for the computation of the transmittance, as can be concluded from Eq. (2).

The optical constants of pure materials are known in literature: Figs. 8(a) and 8(b) display the complex dielectric function of solid Au and pure water, respectively, deduced from experimental data from Ref. 15 for Au and Ref. 16 for water. In the case of a composite material such as NPG having its pores filled with water, the effective dielectric function ε_{eff} can be determined using the BM approach according to the following expression:[12]

$$f_m \frac{\varepsilon_m - \varepsilon_{eff}}{\varepsilon_m + \kappa\varepsilon_{eff}} + f_w \frac{\varepsilon_w - \varepsilon_{eff}}{\varepsilon_w + \kappa\varepsilon_{eff}} = 0. \quad (3)$$

In Eq. (3), f_m and f_w represent the volume fractions of the metal (here Au) and the surrounding medium (here water), respectively; the sum of f_m and f_w is equal to unity. Note that f_m is a measure for the relative density in nanoporous metals, and it emphasizes that f_m changes when features sizes are coarsened. Indeed, we have highlighted above that the growth rate of the ligaments is different from that of the pores; it is obvious in the situation where ligaments growth faster than the pores, that in the limit, the void fraction will approach zero whereas the metal fraction will tend to unity. In our computational work, we have taken into account changes in f_m by assuming that the relative density is proportional to the ratio of the pore size to the ligament diameter (i.e., $f_m \sim 1/\eta$).[7] Further in Eq. (3), ε_m and ε_w are the complex dielectric function of pure Au and water, respectively; we use for this work the experimental data presented in Fig. 8(a) for ε_m and in Fig. 8(b) for ε_w. Finally, κ is the screening parameter depending on the shape of the nanoparticles but also on the orientation of these particles with respect the electric field.[12,13] Some specific values of η are 2 for spherical nanoparticles and $\sim$1 for long nanowires oriented in the direction of the light beam. It is emphasized that η is a critical parameter with respect to the microstructure of the material because it carries information on the shape (i.e., η) of the ligaments. The ligaments in NPG are mostly elongated as depicted by the scanning electron micrographs of Figs. 2(b) and 6(b), which means that these ligaments look like nanorods. In this case, the screening parameter κ is deduced from the depolarization factors P_j,[9] where the index j represents the three axes A, B, and C, with A > B = C (i.e., A is along the longitudinal axis) as follows:[10,12,13]

$$\kappa_j = \frac{1 - P_j}{P_j}, \quad (4)$$

$$P_A = \frac{1-\eta^2}{\eta^2}\left[\frac{1}{2\eta}\ln\left(\frac{1+\eta}{1-\eta}\right) - 1\right], \quad (5)$$

$$P_B = P_C = \frac{1 - P_A}{2}. \quad (6)$$

In Eqs. (5) and (6), the parameter ξ is related to the aspect ratio η of the ligament via the following expression:[10]

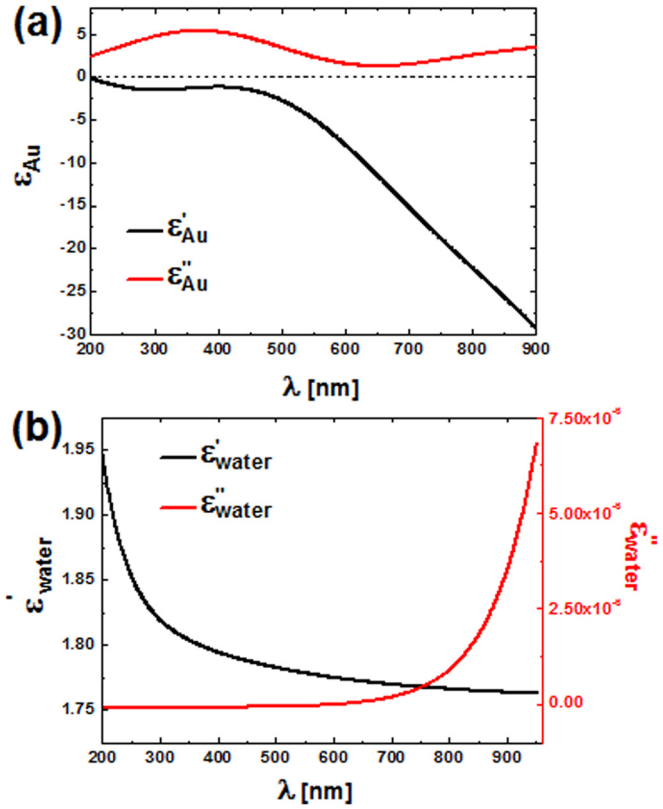

FIG. 8. Complex dielectric function of solid Au (a) and pure water (b) derived from experimental data from Ref. 15 for Au and Ref. 16 for water. The real components are in black, and the imaginary components are in red.

$$\xi^2 = 1 - \frac{1}{\eta^2}. \tag{7}$$

The effective dielectric function ε_{eff} of our composite film (NPG in water) can be derived from the Bruggeman's expression given by Eq. (3). We refer to the Appendix for further details. The complex solutions of Eq. (3) can be written as follows (see for more details Eq. (A9) in the Appendix):

$$\varepsilon_{eff} = \varepsilon'_{eff} + i\varepsilon''_{eff}. \tag{8}$$

A typical solution of Eq. (8), i.e., the effective dielectric function ε_{eff} of our NPG/water hybrid material, is plotted together with the complex dielectric function of Au in Fig. 9(a), when j in Eq. (4) is equal to A, i.e., the principal axis of the ligaments is oriented along the electric field of light; and in Fig. 9(b) when j in Eq. (4) is equal to B or C, i.e., the principal axis of the ligaments is oriented perpendicular to the electric field carried by light. This solution corresponds to an aspect ratio η of 2 for the ligaments.

The effective index of refraction n_{eff} and absorption coefficient k_{eff} are deduced from Eqs. (1) and (8) as follows:

$$\begin{cases} n_{eff}^2 - k_{eff}^2 = \varepsilon'_{eff} \\ 2n_{eff}k_{eff} = \varepsilon''_{eff}, \end{cases} \tag{9}$$

$$n_{eff} = \frac{1}{\sqrt{2}}\sqrt{\varepsilon'_{eff} + \sqrt{\varepsilon'^2_{eff} + \varepsilon''^2_{eff}}}, \tag{10}$$

$$k_{eff} = \frac{sign(\varepsilon''_{eff})}{\sqrt{2}}\sqrt{-\varepsilon'_{eff} + \sqrt{\varepsilon'^2_{eff} + \varepsilon''^2_{eff}}}. \tag{11}$$

The effective index of refraction n_{eff} and absorption coefficient k_{eff} of our NPG/water hybrid material deduced from the solution plotted in Figs. 8(a) and 8(b) are displayed in Figs. 10(a) and 10(b), respectively, together with the index of refraction and absorption coefficient of solid Au. The transmittance of our NPG/water composite film can be computed by replacing n and k in Eq. (2) by n_{eff} and k_{eff} from Eqs. (10) and (11). Typical computed transmittance spectra are plotted in Figs. 11(a) and 11(b) for various ARs ranging from 2.5 to 9.5. In Fig. 11(a), the principal axis of the ligaments is oriented along the electric field of light (longitudinal LSPR). In Fig. 11(b), the principal axis of the ligaments is oriented perpendicular to the electric field of light (transverse LSPR). Our computational results are summarized as follows: (i) A short-wavelength peak appears in the spectrum when the principal axis of the ligaments is oriented perpendicular to the electric field of light (transverse LSPR). (ii) A long-wavelength peak appears in the spectrum when the principal axis of the ligaments is oriented along the electric field of light (longitudinal LSPR). (iii) As the AR approaches unity, both short- and long-wavelength peaks overlap. (iv) When the AR increases, the long-wavelength peak consistently shifts to the red and in the meantime the short-wavelength peak slightly shifts to the blue. (v) When the film thickness d in Eq. (2) is varied, the amplitude (intensity) of the spectrum changes, but the positions of the peaks are not affected, i.e., the peaks do not shift upon increasing

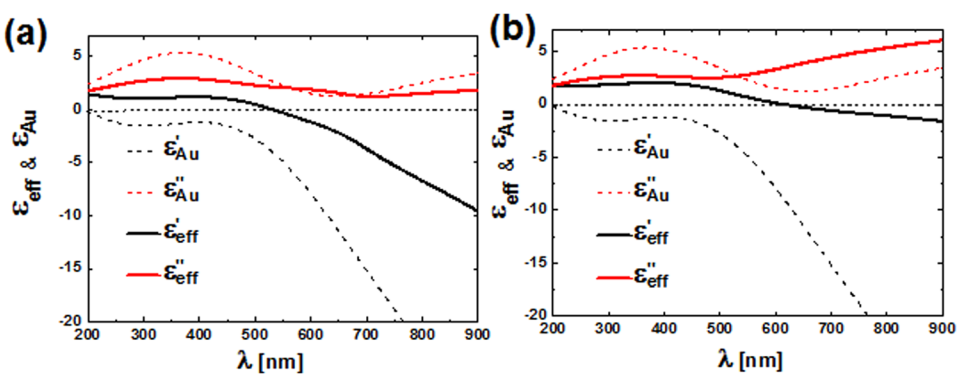

FIG. 9. Typical effective dielectric function of the NPG/water composite material for an aspect ratio equal to 2, plotted together with the complex dielectric function of solid Au. (a) The principal axis of the ligaments is oriented along the electric field carried by light (i.e., j = A in Eq. (4)). (b) The principal axis of the ligaments is oriented perpendicular to the electric field carried by light (i.e., j = B, C in Eq. (4)). Here also the real components are in black, and the imaginary parts are in red.

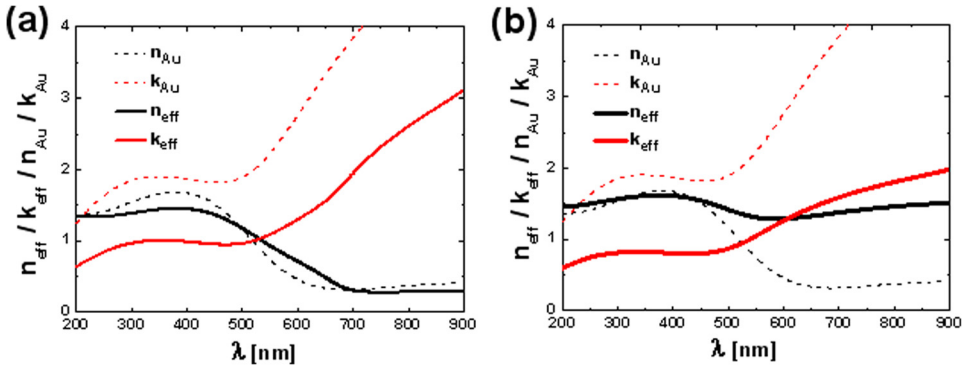

FIG. 10. Typical effective index of refraction and absorption coefficient of the NPG/water hybrid material for an aspect ratio equal to 2. The optical constants of solid Au are also plotted for the sake of comparison. (a) The principal axis of the ligaments is oriented along the electric field. (b) The principal axis of the ligaments is oriented perpendicular to the electric field.

thickness of the film. These computational results are in good agreement with our experimental findings.

The work presented in this article shows that the short-wavelength peak in NPG films does not originate from the resonant absorption in the films.[1] The origin of the two plasmonic modes in disordered NPG films points toward the longitudinal LSPR in the ligaments,[10] for the long-wavelength peak, and transverse LSPR in the ligaments,[10] for the short-wavelength peak.

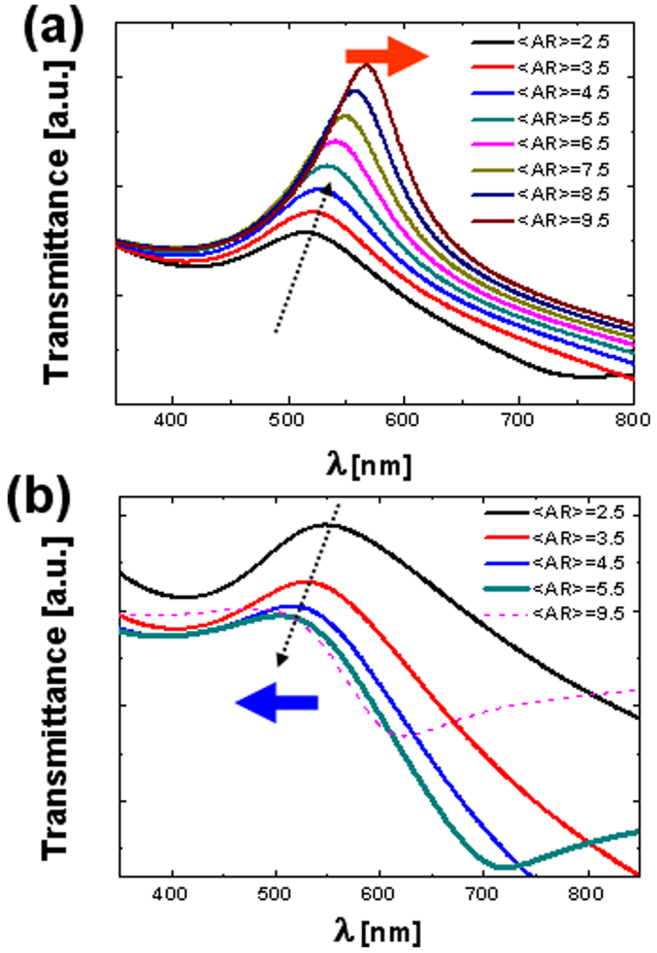

FIG. 11. Computed transmittance spectra plotted for various aspect ratios AR ranging from 2.5 to 9.5. (a) Principal axis of the ligaments oriented along the electric field of light (longitudinal LSPR). The peaks shift to the red. (b) Principal axis of the ligaments is oriented perpendicular to the electric field of light (transverse LSPR). The peaks shift slightly to the blue.

V. CONCLUSION

Light transmission in free-standing nanoporous gold films was systematically investigated as a function of the feature size in the film. It appears from both experimental and computational results that the shifting behavior of the plasmonic peaks can be described by taking the ratio of ligament to the pore sizes as the relevant parameter, rather than the size of either ligaments or pores. As in the case of rod-shape metallic nanoparticles, the origin of the two plasmonic modes in free-standing NPG films is attributed to the longitudinal and transverse LSPR in the ligaments.

ACKNOWLEDGMENTS

Financial support from the Netherlands Organization of Research (NWO-The Hague) and the Zernike Institute for Advanced Materials is gratefully acknowledged.

APPENDIX: CALCULATION OF EFFECTIVE DIELECTRIC CONSTANTS

The BM expression in Eq. (3) was recast into a quadratic equation with as variable ε_{eff} (Ref. 10)

$$\kappa\varepsilon_{eff}^2 - [\varepsilon_m(f_m\kappa - f_w) + \varepsilon_w(f_w\kappa - f_m)]\varepsilon_{eff} - \varepsilon_m\varepsilon_w. \quad \text{(A1)}$$

The two possible solutions of that quadratic equation are given by

$$\varepsilon_{eff} = \frac{-\beta \pm \sqrt{\Delta}}{2\kappa}. \quad \text{(A2)}$$

In Eq. (A2), β is the first order term from the quadratic equation and Δ is the discriminant. The square root of Δ can be derived as follows:

$$\sqrt{\Delta} = (x + iy), \quad \text{(A3)}$$

$$\Delta = \Delta' + i\Delta'', \quad \text{(A4)}$$

$$\Delta' + i\Delta'' = (x + iy)^2, \quad \text{(A5)}$$

$$x = \frac{1}{\sqrt{2}}\sqrt{\Delta' + \sqrt{\Delta'^2 + \Delta''^2}}, \quad \text{(A6)}$$

$$y = \frac{sign(\Delta'')}{\sqrt{2}}\sqrt{-\Delta' + \sqrt{\Delta'^2 + \Delta''^2}}, \quad \text{(A7)}$$

$$sign(\Delta'') = \begin{cases} 1 if \Delta'' > 0 \\ -1 if \Delta'' < 0. \end{cases} \quad \text{(A8)}$$

In the above expressions, Δ' and Δ'' represent the real and imaginary part of the discriminant; x and y represent the real and imaginary part of the square root of that discriminant.

The complex solutions of the quadratic expression in Eq. (A1) can be written as follows:

$$\varepsilon_{eff} = \varepsilon'_{eff} + i\varepsilon''_{eff} = \frac{(-\beta' \pm x)}{2\kappa} + i\frac{(-\beta'' \pm y)}{2\kappa}. \quad \text{(A9)}$$

In Eq. (A9), β' and β'' represent the real and imaginary part of β. Note the existence of two possible solutions for the effective dielectric function as given by the two values of the real part ($\pm x$) and the imaginary ($\pm y$) of the square root of Δ. The consistent solution ε_{eff} was obtained with $+x$ and $+y$.

[1]T. W. Ebbesen, H. J. Lezec, H. F. Ghaemi, T. Thio, and P. A. Wolff, Nature **391**, 667 (1998).
[2]L. Martín-Moreno, F. J. García-Vidal, H. J. Lezec, K. M. Pellerin, T. Thio, J. B. Pendry, and T. W. Ebbesen, Phys. Rev. Lett. **86**, 1114 (2001).
[3]X. Lang, L. Qian, P. Guan, J. Zi, and M. Chen, Appl. Phys. Lett. **98**, 093701 (2011).
[4]S. Coyle, M. C. Netti, J. J. Baumberg, M. A. Ghanem, P. R. Birkin, P. N. Bartlett, and D. M. Whittaker, Phys. Rev. Lett. **87**, 176801 (2001).
[5]T. V. Teperik, V. V. Popov, and F. J. G. de Abajo, Phys. Solid State **47**, 178 (2005).
[6]E. Detsi, S. Punzhin, J. Rao, P. R. Onck, and J. T. M. De Hosson, ACS Nano **6**, 3734 (2012).
[7]E. Detsi, E. De Jong, A. Zinchenko, Z. Vuković, I. Vuković, S. Punzhin, K. Loos, G. ten Brinke, H. A. De Raedt, P. R. Onck, and J. T. M. De Hosson, Acta Mater. **59**, 7488 (2011).
[8]E. Detsi, S. Punzhin, P. R. Onck, and J. T. M. De Hosson, J. Mater. Chem. **22**, 4588 (2012).
[9]E. Detsi, M. van de Schootbrugge, S. Punzhin, P. R. Onck, and J. T. M. De Hosson, Scr. Mater. **64**, 319 (2011).
[10]S. Link and M. A. El-Sayed, Int. Rev. Phys. Chem. **19**, 409 (2000).
[11]M. Hu, J. Chen, Z.-Y. Li, L. Au, G. V. Hartland, X. Li, M. Marquez, and Y. Xia, Chem. Soc. Rev. **35**, 1084 (2006).
[12]C. A. Foss, Jr., M. J. Tierney, and C. R. Martin, J. Phys. Chem. **96**, 9001 (1992).
[13]C. A. Foss, Jr., G. L. Hornyak, J. A. Stockert, and C. R. Martin, J. Phys. Chem. **98**, 2963 (1994).
[14]D. E. Aspnes, E. Kinsbron, and D. D. Bacon, Phys. Rev. B **21**, 3290 (1980).
[15]P. B. Johnson and R. W. Christy, Phys. Rev. B **6**, 4370 (1972).
[16]G. M. Hale and M. R. Querry, Appl. Op. **12**, 555 (1973).